

First-Principles AI finds crystallization of fractional quantum Hall liquids

Ahmed Abouelkomsan^{1,*} and Liang Fu^{1,†}

¹*Department of Physics, Massachusetts Institute of Technology, Cambridge, MA-02139, USA*

When does a fractional quantum Hall (FQH) liquid crystallize? Addressing this question requires a framework that treats fractionalization and crystallization on equal footing, especially in strong Landau-level mixing regime. Here, we introduce MagNet, a self-attention neural-network variational wavefunction designed for quantum systems in magnetic fields on the torus geometry. We show that MagNet provides a *unifying* and expressive ansatz capable of describing both FQH states and electron crystals within the same architecture. Trained solely by energy minimization of the microscopic Hamiltonian, MagNet discovers topological liquid and electron crystal ground states across a broad range of Landau-level mixing. Our results highlight the power of first-principles AI for solving strongly interacting many-body problems and finding competing phases without external training data or physics pre-knowledge.

Introduction — When does a fractional quantum Hall (FQH) liquid crystallize? This question lies at the heart of the competition between topological order and charge ordering in two-dimensional electron systems and has motivated numerous theoretical and numerical efforts [1–6]. It is also directly relevant experimentally [7–11]: by tuning the carrier density and magnetic field, experiments can access both FQH and Wigner crystal regimes in high-mobility two dimensional semiconductors [12]. Addressing the competition between fractionalization and crystallization in an unbiased manner remains an outstanding challenge, because an interacting 2DEG in a magnetic field features an infinite ladder of Landau levels and strong electron correlation. Quantum Monte Carlo faces severe complex phase problem; and density matrix renormalization group suffers from discretization errors due to Landau level truncation. As a result, much of our understanding relies on trial wave functions that are tailor made for FQH liquids and Wigner crystals separately, making it difficult to determine the phase boundary in an unbiased way.

In recent years, neural-network quantum states [13–15] have emerged as a powerful new class of variational wave functions and have attained accurate results in continuum Fermi systems. Here the networks are trained directly optimized by minimizing the variational energy of the microscopic Hamiltonian. Remarkably, recent studies [16–20] have found that ground states of vastly different quantum phases—ranging from Fermi liquids and Wigner crystals to fractional Hall states and superconductors—can all be captured within a single neural architecture; fundamentally distinct quantum states simply correspond to different values of network parameters.

This unprecedented expressive power has further motivated the development of *universal* Fermi networks that are provably capable of representing any fermionic wave function at sufficient network size [21]. Recently, a universal architecture—“Fermi Sets”—has been introduced

[22], which is mathematically proven to be universal approximators of continuous fermionic wave functions while retaining physical interpretability. Universal Fermi networks of sufficiently large size can in principle solve many-electron Schrodinger equations to arbitrary accuracy. This opens vast opportunities for *first-principles AI* in quantum chemistry, condensed matter physics, material science and quantum computing.

In this work, we develop a self-attention Fermi network to solve the strongly correlated problem of two-dimensional interacting electrons in a magnetic field, where fractionalization competes with crystallization. In contrast to previous neural-network variational studies [16, 23], we work on the torus geometry, which is free of boundary effects and naturally accommodates both topological fluids and crystalline order in an unbiased way. A key innovation is our construction of a real-space neural wave function that exactly respects the nontrivial boundary conditions imposed by magnetic translations while remaining extremely expressive. In particular, our network allows for general, intricate phase structures far beyond those of standard quantum Hall model wave functions.

Using this unifying architecture, we obtain accurate ground-state energies and wave functions across the entire range of Landau-level (LL) mixing, from weak to strong. The same neural network discovers both FQH liquids and electron crystals directly from the microscopic Hamiltonian, without being supplied with any physics knowledge, such as Landau levels, Laughlin states, flux attachment, or crystalline order. All information about fractionalization and crystallization is extracted a posteriori from the wavefunction learned by the network through energy minimization alone. In this sense, our work realizes a genuinely first-principles AI solver for this paradigmatic strongly correlated problem.

Beyond verifying known phases in the limit of weak and strong LL mixing, our work provides, for the first time, a unified solution across the FQH-to-crystal topological quantum phase transition, within a single family of variational wavefunctions. This enables us to follow the evolution of correlation functions and structure fac-

* ahmed95@mit.edu

† liangfu@mit.edu

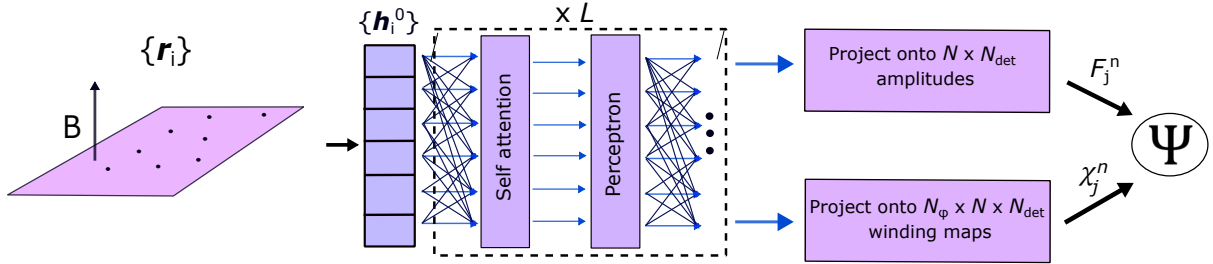


FIG. 1. Schematic illustration of the MagNet architecture: Electron coordinates (in the presence of magnetic field) are mapped to higher dimensional feature space which is passed to L layers of successive self-attention and multi-layer perceptron blocks. The final output undergo two different projections to form the generalized orbitals (6) which build the full variational ansatz. For simplicity, we show a plane pierced by a magnetic field but our ansatz is designed for the torus geometry.

tors and locate the onset of crystalline order.

More broadly, our study highlights the power of first-principles AI as a general-purpose tool for quantum matter, capable of exploring phase diagrams, discovering unexpected correlated phases, and offering new microscopic insights into the organizing principles of strongly interacting electrons.

Setup— Our starting point is the standard problem of two dimensional electrons subject to an external magnetic field and interacting with Coulomb potential. The many-body Hamiltonian of N particles reads,

$$H = \sum_i \frac{(-i\hbar\nabla_i + e\mathbf{A}(\mathbf{r}_i))^2}{2m} + \frac{1}{2} \sum_{i \neq j} \frac{e^2}{4\pi\epsilon|\mathbf{r}_i - \mathbf{r}_j|} \quad (1)$$

where $\mathbf{A}(\mathbf{r})$ is the vector potential of the magnetic field $\mathbf{B} = \nabla \times \mathbf{A}(\mathbf{r})$. This problem is governed by two energy scales, the kinetic energy scale $K = \hbar\omega_c$ which sets the gap between the (infinite) ladder of flat Landau levels with $\omega_c = eB/m$ the cyclotron frequency and interaction scale $U = e^2/4\pi\epsilon\ell_B$ which sets the strength of the Coulomb repulsion in terms of the magnetic length $\ell_B = \sqrt{\hbar/eB}$. The many-body ground state at filling factor ν is therefore controlled by the ratio of the two, $\kappa = U/K \propto 1/\sqrt{B}$ which describes the amount of Landau level mixing. κ is related to the dimensionless interaction strength parameter $r_s = 1/\sqrt{\pi a_B^2 n}$ through $\kappa = r_s \sqrt{\nu/2}$ where $a_B = \hbar^2/e^2 m$ is the Bohr radius and n is the density. Experimentally, for a given magnetic field, κ is material-dependent and can become very large in materials with heavy effective mass, such as hole doped GaAs, ZnO or transition metal dichalcogenides (TMDs) [9, 12, 24–27].

Focusing on $\nu < 1$, the physics in the limit $\kappa \rightarrow 0$ is confined to the lowest Landau level where fractional quantum Hall liquids arise at various fillings, while increasing κ drives substantial Landau-level mixing and can quantitatively change the ground state. In particular, when $\kappa \rightarrow \infty$, interactions dominate over kinetic energy and the ground state becomes a classical Wigner crystal. At intermediate values of κ , the system lies in a genuinely nonperturbative regime, and the FQH

liquid competes with various possible charge-ordered states such as Wigner crystals, composite fermion crystals [2, 28–32], or Hall crystals [33]. Resolving this competition requires a method that can treat strong Landau-level mixing, while remaining unbiased with respect to competing states.

To proceed, we work on the torus geometry which is defined by two basis vectors \mathbf{L}_1 and \mathbf{L}_2 and is pierced by a magnetic field whose total flux is quantized to an integer number N_ϕ of flux quanta, fixed by $|\mathbf{L}_1 \times \mathbf{L}_2| = 2\pi N_\phi \ell_B^2$. The torus provides a particularly favorable geometry for studying competing quantum phases. Unlike the disk, it has no physical edge and therefore avoids boundary effects and edge reconstruction [34]. Compared to the sphere, it also avoids curvature and the associated topological shift [35] that can complicate finite-size comparisons across different phases. Additionally, the torus naturally accommodates translational symmetry, making it well suited not only for uniform quantum Hall liquids but also for charge-ordered phases such as Wigner crystals, whose periodicity can be embedded commensurately in the torus supercell.

NN wavefunction— To comply with the periodicity of the torus, any wavefunction has to transform under translation of a single particle as [36],

$$\Psi(\mathbf{r}_1, \dots, \mathbf{r}_i + \mathbf{L}, \dots, \mathbf{r}_N) = e^{i\varphi} e^{i\xi_{\mathbf{L}}(\mathbf{r}_i)} \Psi(\mathbf{r}_1, \dots, \mathbf{r}_N) \quad (2)$$

where $\xi_{\mathbf{L}}(\mathbf{r}_i)$ is the magnetic phase determined by $\nabla \xi_{\mathbf{L}}(\mathbf{r}_i) = \frac{e}{\hbar} [\mathbf{A}(\mathbf{r}_i + \mathbf{L}) - \mathbf{A}(\mathbf{r}_i)]$ and $\mathbf{L} = m\mathbf{L}_1 + n\mathbf{L}_2$ is a generic torus vector with integers m and n . φ is an additional twist phase corresponding to threading flux through the handles of the torus, implemented by a constant vector potential.

Importantly, the condition (2) implies that the net winding \mathcal{W} of the wavefunction as a function of one particle coordinate \mathbf{r}_i (while fixing the remaining $N - 1$ particles $\{\mathbf{r}_{\neq i}\}$) has to be $\mathcal{W} = N_\phi$ [37, 38]. This net winding constraint requires the wavefunction to contain phase singularities on the torus—i.e., vortices where Ψ vanishes and its phase winds. In general, the wavefunction may host both vortices and antivortices, but their contributions must sum to the same net winding: the to-

tal winding (vortices counted with positive charge minus antivortices counted with negative charge) is fixed to N_ϕ .

Our variational wavefunction for the many-body ground state is given by,

$$\Psi_{\{\theta\}}(\{\mathbf{r}_i\}) = e^{\mathcal{J}(\{\mathbf{r}_i\})} \sum_n^{N_{\text{det}}} \det[\phi_j^n(\mathbf{r}_i; \{\mathbf{r}_{\neq i}\})] \quad (3)$$

where $\phi_j^n(\mathbf{r}_i; \{\mathbf{r}_{\neq i}\})$ is a generalized many-body orbital for the i -th particle that depends on the coordinates of the remaining particles $\mathbf{r}_{\neq i}$. $\{\theta\}$ denotes the variational parameters of the ansatz. $\mathcal{J}(\{\mathbf{r}_i\})$ is a periodic symmetric Jastrow factor, $\mathcal{J}(\mathbf{r}_1, \dots, \mathbf{r}_i + \mathbf{L}, \dots, \mathbf{r}_N) = \mathcal{J}(\mathbf{r}_1, \dots, \mathbf{r}_N)$, to enforce electron cusp conditions for long-range Coulomb interactions. However, the existence of a Jastrow factor here is not generally needed and we obtained similar results without it.

To respect fermionic antisymmetry, ϕ_j^n has to be permutation *equivariant* in the coordinates $\{\mathbf{r}_{\neq i}\}$ [14, 17]. Moreover, to enforce magnetic boundary condition (2), ϕ_j^n transforms under translations of \mathbf{r}_i as,

$$\phi_j^n(\mathbf{r}_i + \mathbf{L}, \{\mathbf{r}_{\neq i}\}) = e^{i\varphi} e^{i\xi_{\mathbf{L}}(\mathbf{r}_i)} \phi_j^n(\mathbf{r}_i; \{\mathbf{r}_{\neq i}\}) \quad (4)$$

and is periodic in the rest $\{\mathbf{r}_{\neq i}\}$

$$\phi_j^n(\mathbf{r}_i, \{\dots, \mathbf{r}_k + \mathbf{L}, \dots, \mathbf{r}_l, \dots\}) = \phi_j^n(\mathbf{r}_i; \{\mathbf{r}_{\neq i}\}) \quad (5)$$

for $k, l, \dots, \neq i$. A sum of determinants over ϕ_j^n as in the ansatz (3) automatically satisfies the condition (2) and therefore represents a physically valid wavefunction on the torus.

Furthermore, ϕ_j^n is factorized into a product,

$$\phi_j^n(\mathbf{r}_i; \{\mathbf{r}_{\neq i}\}) = \chi_j^n(\mathbf{r}_i; \{\mathbf{r}_{\neq i}\}) F_j^n(\mathbf{r}_i; \{\mathbf{r}_{\neq i}\}) \quad (6)$$

where F_j^n is a periodic function in all coordinates, $F_j^n(\mathbf{r}_1, \dots, \mathbf{r}_i + \mathbf{L}, \mathbf{r}_N) = F_j^n(\mathbf{r}_1, \dots, \mathbf{r}_N)$ while χ_j^n transforms similar to ϕ_j^n (Equations (4) and (5)).

To impose a net winding of N_ϕ , the core innovation of our ansatz is to parametrize χ_j^n in terms of a product over N_ϕ terms,

$$\chi_j^n(\mathbf{r}_i; \{\mathbf{r}_{\neq i}\}) = \prod_{\alpha=1}^{N_\phi} f(z_i - \eta_j^{(n,\alpha)}(\{\mathbf{r}\})) \quad (7)$$

where $f(z_i)$ is a gauge-dependent quasi-periodic function in the coordinate z_i with net winding $\mathcal{W} = +1$ in the fundamental domain of the torus spanned by \mathbf{L}_1 and \mathbf{L}_2 and $z_i = x_i + iy_i$ is the complex coordinate of \mathbf{r}_i . For our purposes, the function $f(z_i - \eta)$ vanishes when $z_i = \eta$. Importantly, $\eta_j^{(n,\alpha)}(\{\mathbf{r}\})$ here is a *learnable* periodic and symmetric many-body function in *all* coordinates. The zeros of χ_j^n and their windings are determined through the solutions of $z_i = \eta_j^{(n,\alpha)}(\{\mathbf{r}\})$. For this reason, we refer to $\eta_j^{(n,\alpha)}(\{\mathbf{r}\})$ as a winding map.

We note that if the winding maps $\{\eta\}$ in (7) are taken to be fixed parameters (no dependence on $\{\mathbf{r}\}$), then

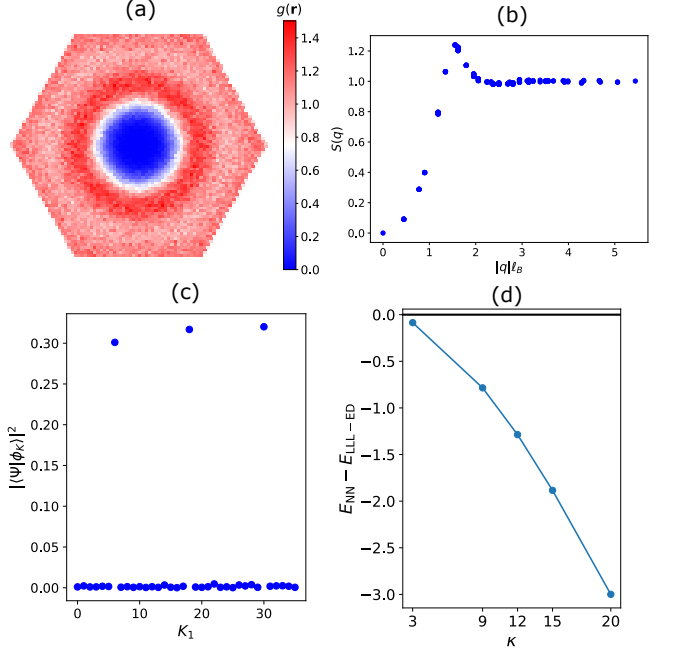


FIG. 2. (a) Pair correlation function $g(\mathbf{r})$ at $\kappa = 3.0$. (b) The structure factor $S(\mathbf{q})$ along a line cut at $\kappa = 3.0$. (c) The overlap $|\langle \Psi | \Phi_{K_1} \rangle|^2$ of the optimized wavefunction Ψ at $\kappa = 3.0$ with its projection Φ_{K_1} defined as the eigenstates of CM magnetic translation operator along L_1 . (d) Comparison of the variational energy of the NN ansatz E_{NN} (in units of $\hbar\omega_c$) against the energies obtained from exact diagonalization $E_{\text{LLL-ED}}$ projected onto the lowest Landau level for various values of κ . All calculations are performed at filling $\nu = 1/3$ ($N = 12$ and $N_\phi = 36$) on a hexagonal torus with equal aspect ratio.

χ_j^n reduces to the single particle lowest Landau level (LLL) wavefunction which is specified by N_ϕ vortices and is holomorphic (up to a Gaussian factor) [37, 39]. In contrast, allowing $\{\eta\}$ to depend on all particle coordinates—including \mathbf{r}_i itself—generically introduces \bar{z} -dependence, so that χ_j^n becomes non-holomorphic. Together with the additional periodic factor F_j^n , this non-holomorphic structure enables the full many-body ansatz to represent states residing outside the LLL. Crucially, by promoting the zeros of the generalized orbitals to be many-body trainable functions, the variational ansatz can capture non-trivial phase effects in a correlated manner.

To proceed, we work in the symmetric gauge, $A(\mathbf{r}) = B_0(\hat{z} \times \mathbf{r})/2$, where B_0 denotes the uniform component of the magnetic field. In this gauge, the magnetic translation phase takes the form

$$e^{i\xi_{\mathbf{L}}(\mathbf{r})} = (-1)^{mn+m+n} e^{i(\mathbf{r} \times \mathbf{L})/2\ell_B^2} \quad (8)$$

for $\mathbf{L} = m\mathbf{L}_1 + n\mathbf{L}_2$. We choose $f(z)$ in Eq. (7) to be the modified Weierstrass sigma function [40–42]. In this representation, the sum of the winding maps, $\bar{\eta}_j^{(n)} = (\sum_\alpha \eta_j^{(n,\alpha)}) \bmod (L_x + iL_y)$, fixes the twist phase

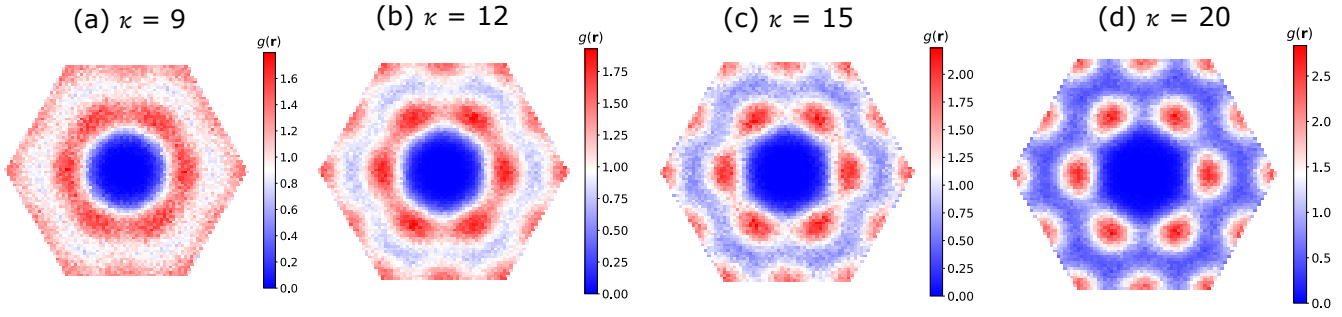


FIG. 3. Pair correlation function $g(\mathbf{r})$ at $\nu = 1/3$ for various values of the Landau level mixing parameter κ . All calculations are performed with $N = 12$ and $N_\phi = 36$ on a hexagonal torus with equal aspect ratio.

φ in Eq. (4). Throughout, we set $\varphi = 0$ by imposing the constraint $\bar{\eta}_j^{(n)} = 0$ [36].

Next, we represent the generalized orbitals ϕ_j^n with a deep neural network (Fig. 1) based on the self-attention mechanism [17, 43]. As initial input, the NN takes the *periodized* coordinates of the particles on the torus [$\sin(\mathbf{G}_a \cdot \mathbf{r}_i)$ and $\cos(\mathbf{G}_a \cdot \mathbf{r}_i)$] where $\mathbf{G}_{a=1,2}$ are the reciprocal lattice vectors, i.e., $\mathbf{G}_a \cdot \mathbf{L}_b = 2\pi\delta_{ab}$. These inputs are then passed through L layers of successive self-attention and perceptron blocks. The final output of the NN is projected to construct the amplitudes F_j^n and the winding maps $\eta_j^{(n,\alpha)}$ of χ_j^n to form the generalized orbitals ϕ_j^n . The parameters of the ansatz $\{\theta\}$ are optimized through energy minimization to yield the final ansatz (3). Our construction is distinct from very recent work [44] in several key aspects. Rather than a linear combination of single particle orbitals, the quasi-periodic function χ_j^n (7) is parametrized by its zeros as determined by winding maps $\{\eta\}$ that depend on *all* particle coordinates, leading to enhanced expressivity. Moreover, as we shall demonstrate below, our parametrization successfully captures fractional quantum Hall liquids without additional neural-network Jastrow factor. We refer the reader to the supplemental material [36] for comprehensive details about the architecture and the optimization.

Results — To test the validity of our ansatz, we apply it to the Hamiltonian (1) at filling factor $\nu = 1/3$. At $\kappa = 3.0$, the optimized neural-network wavefunction exhibits hallmarks of a fractional quantum Hall liquid. Fig. 2(a) shows the pair correlation function $g(\mathbf{r}) = \frac{A}{N^2} \langle \sum_{i \neq j} \delta^2(\mathbf{r} - \mathbf{r}_i + \mathbf{r}_j) \rangle$ and Fig. 2(b) shows the structure factor $S(\mathbf{q}) = \frac{1}{N} \langle \rho_{\mathbf{q}} \rho_{-\mathbf{q}} \rangle$ with the density operator $\rho_{\mathbf{q}} = \sum_i e^{i\mathbf{q} \cdot \mathbf{r}_i}$. In both cases, the density correlations in the ground state are liquid-like indicating the absence of crystalline order in the ground state.

Next, we probe the existence of topological order by demonstrating the expected topological ground state degeneracy [20]. To this end, we decompose the optimized many-body wavefunction $\Psi(\{\mathbf{r}\})$ onto center of mass (CM) momentum sectors $\Phi_K(\{\mathbf{r}\})$, defined as eigenstates of the CM magnetic translation operator $T_{\text{CM}}(n\mathbf{L}_1/N_\phi)$ with $n = 0, \dots, N_\phi - 1$. As shown in Fig. 2(c), the

resulting state carries nonzero weight in only three CM momentum sectors, matching precisely the sectors of the $\nu = 1/3$ Laughlin state for the same finite-size geometry. Taken together, our findings establishes the ability of the NN ansatz to discover a fractional quantum Hall liquid on the torus geometry.

To further corroborate the effectiveness of our ansatz in capturing strong Landau-level mixing, we compare its energy against lowest-Landau-level (LLL) projected exact diagonalization (ED) in Fig. 2(d). We find that the NN achieves consistently lower variational energies than the corresponding ED energies. This highlights a key advantage of our approach: for this system size ($N_\phi = 36$), ED is restricted to the LLL and can only capture a FQH liquid regardless of κ , whereas our real-space NN ansatz naturally incorporates Landau-level mixing without truncation and allows for competing phases.

To address whether strong Landau level mixing can destabilize the fractional quantum Hall liquid, we use our unified NN ansatz to study the evolution of the many-body ground state as a function of κ . As shown in Fig. 3, the pair-correlation function $g(\mathbf{r})$ evolves from being featureless and liquid-like to exhibiting well-developed spatial modulations as κ increases, signaling a transition toward a crystalline phase.

To assess whether these correlations correspond to true long-range crystalline order in the thermodynamic limit, we perform a finite-size scaling of the structure factor $S(\mathbf{q})$. First, we find $S(\mathbf{q})$ to have maximum value at $\mathbf{q} = \mathbf{K}$ for various values of κ with \mathbf{K} being the ordering wavevector of a crystal with one electron per unit cell. However, as shown in Fig. 4, the magnitude of this peak $S(\mathbf{K})$ exhibits only a small enhancement with increasing particle number N for $\kappa = 12$ and $\kappa = 15$, suggesting at most incipient charge order at these values. In contrast, for $\kappa = 3$ and $\kappa = 9$, $S(\mathbf{K})$ does not grow with N and is nearly constant, consistent with a FQH liquid.

Discussion — In this paper, we have developed a self-attention neural network variational wavefunction to study quantum systems subject to magnetic fields on the

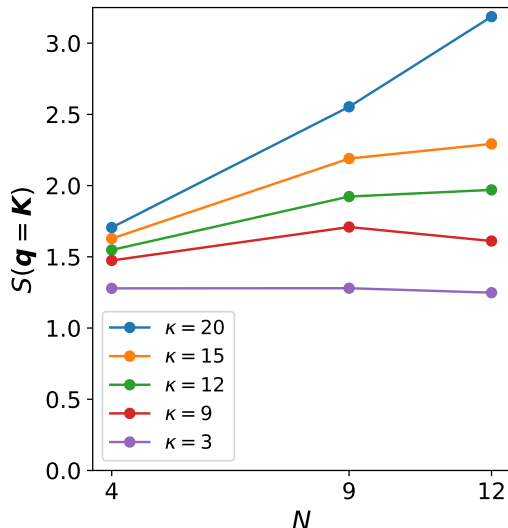


FIG. 4. Structure factor $S(\mathbf{q})$ evaluated at the ordering wavevector $\mathbf{q} = \mathbf{K}$ corresponding to a crystal with one electron per unit cell, plotted as a function of particle number N for various values of κ . The reported $S(\mathbf{q} = \mathbf{K})$ is rotationally averaged over the six C_6 -related ordering wavevectors.

torus geometry. We have shown that our single ansatz captures both fractional quantum Hall liquids and crystals in a unified manner. While we have presented evidence of pronounced crystalline correlations with increasing Landau level mixing, the full nature of the crystal phase is yet to be established. Apart from topologically trivial Wigner crystal or the composite fermion crystal, an intriguing possibility is the realization of (integer or fractional) Hall crystal [33, 45–47], a state that spontaneously break magnetic translational symmetry but has quantized Hall conductance.

Earlier numerical work [3] suggested that the $\nu = 1/3$ FQH liquid undergoes a transition to a crystalline phase at Landau-level mixing, around $\kappa \approx 9$ (corresponding to $r_s \approx 22$). In contrast, more recent studies based on fixed-

phase diffusion Monte Carlo (DMC) [2]—where the complex phase of the trial state is constrained to be that of a composite-fermion wavefunction—did not find crystallization of the $\nu = 1/3$ FQH liquid up to the largest mixing strength considered, $\kappa = 18$ ($r_s \approx 44$). In comparison with these results, our unbiased variational Monte Carlo results—obtained within a single unified ansatz and based on the system sizes accessible here—indicate that long-range crystalline order emerges between $\kappa = 15$ ($r_s \approx 37$) and $\kappa = 20$ ($r_s \approx 49$) (cf. Fig. 4).

The development of a neural-network ansatz that can treat arbitrary Landau-level mixing opens a powerful route to studying a wide range of quantum Hall problems in an unbiased, first-principles manner. While we have focused on $\nu = 1/3$, a natural next step is to apply this framework across a broader set of filling factors to investigate the competition between liquid phases—including incompressible FQH states and compressible composite-fermion Fermi liquids—and crystalline order.

Finally, our neural-network ansatz is naturally suited to problems with spatially non-uniform magnetic fields or external modulations [48], such as moiré systems—for example, twisted transition-metal dichalcogenides—where the moiré potential generates emergent spatially modulated magnetic fields [49–51].

Acknowledgements— We are grateful to Aidan Reddy, Timothy Zaklama and Filippo Gaggioli for useful discussions and related collaborations. We thank Timothy Zaklama for coining the NN architecture name and acknowledge insightful discussions with Max Geier, Daniele Guerci and Pierre-Antoine Graham. This work was supported by a Simons Investigator Award from the Simons Foundation. A. A. was supported by the Knut and Alice Wallenberg Foundation (KAW 2022.0348). This work made use of resources provided by subMIT at MIT Physics. The authors acknowledge the MIT Office of Research Computing and Data for providing high performance computing resources that have contributed to the research results reported within this paper.

[1] G. Ortiz, D. Ceperley, and R. Martin, New stochastic method for systems with broken time-reversal symmetry: 2d fermions in a magnetic field, *Physical review letters* **71**, 2777 (1993).

[2] J. Zhao, Y. Zhang, and J. Jain, Crystallization in the fractional quantum hall regime induced by landau-level mixing, *Physical review letters* **121**, 116802 (2018).

[3] R. Price, P. Platzman, and S. He, Fractional quantum hall liquid, wigner solid phase boundary at finite density and magnetic field, *Physical review letters* **70**, 339 (1993).

[4] P. Platzman and R. Price, Quantum freezing of the fractional quantum hall liquid, *Physical review letters* **70**, 3487 (1993).

[5] X. Zhu and S. G. Louie, Wigner crystallization in the fractional quantum hall regime: A variational quantum monte carlo study, *Physical review letters* **70**, 335 (1993).

[6] W. He, T. Cui, Y. Ma, C. Chen, Z. Liu, and G. Zou, Phase boundary between the fractional quantum hall liquid and the wigner crystal at low filling factors and low temperatures: A path integral monte carlo study, *Physical Review B—Condensed Matter and Materials Physics* **72**, 195306 (2005).

[7] M. Santos, Y. Suen, M. Shayegan, Y. Li, L. Engel, and D. Tsui, Observation of a reentrant insulating phase near the $1/3$ fractional quantum hall liquid in a two-dimensional hole system, *Physical review letters* **68**, 1188 (1992).

[8] M. Santos, J. Jo, Y. Suen, L. Engel, and M. Shayegan, Effect of landau-level mixing on quantum-liquid and solid states of two-dimensional hole systems, *Physical Review*

B **46**, 13639 (1992).

[9] D. Maryenko, A. McCollam, J. Falson, Y. Kozuka, J. Bruin, U. Zeitler, and M. Kawasaki, Composite fermion liquid to wigner solid transition in the lowest landau level of zinc oxide, *Nature communications* **9**, 4356 (2018).

[10] W. Pan, G. Csáthy, D. Tsui, L. Pfeiffer, and K. West, Transition from a fractional quantum hall liquid to an electron solid at landau level filling $\nu = 1/3$ in tilted magnetic fields, *Physical Review B—Condensed Matter and Materials Physics* **71**, 035302 (2005).

[11] Y.-C. Tsui, M. He, Y. Hu, E. Lake, T. Wang, K. Watanabe, T. Taniguchi, M. P. Zaletel, and A. Yazdani, Direct observation of a magnetic-field-induced wigner crystal, *Nature* **628**, 287 (2024).

[12] J. Pack, Y. Guo, Z. Liu, B. S. Jessen, L. Holtzman, S. Liu, M. Cothrine, K. Watanabe, T. Taniguchi, D. G. Mandrus, et al., Charge-transfer contacts for the measurement of correlated states in high-mobility wse2, *Nature Nanotechnology* **19**, 948 (2024).

[13] G. Carleo and M. Troyer, Solving the quantum many-body problem with artificial neural networks, *Science* **355**, 602 (2017).

[14] D. Pfau, J. S. Spencer, A. G. Matthews, and W. M. C. Foulkes, Ab initio solution of the many-electron schrödinger equation with deep neural networks, *Physical review research* **2**, 033429 (2020).

[15] D. Luo and B. K. Clark, Backflow transformations via neural networks for quantum many-body wave functions, *Physical review letters* **122**, 226401 (2019).

[16] Y. Teng, D. D. Dai, and L. Fu, Solving the fractional quantum hall problem with self-attention neural network, *Physical Review B* **111**, 205117 (2025).

[17] M. Geier, K. Nazaryan, T. Zaklama, and L. Fu, Self-attention neural network for solving correlated electron problems in solids, *Physical Review B* **112**, 045119 (2025).

[18] C.-T. Li, T. Ong, M. Geier, H. Lin, and L. Fu, Attention is all you need to solve chiral superconductivity, *arXiv preprint arXiv:2509.03683* (2025).

[19] K. Nazaryan, F. Gaggioli, Y. Teng, and L. Fu, Artificial intelligence for quantum matter: Finding a needle in a haystack, *arXiv preprint arXiv:2507.13322* (2025).

[20] A. Abouelkomans, M. Geier, and L. Fu, Topological order in deep state, *arXiv preprint arXiv:2512.01863* (2025).

[21] L. Fu, A minimal and universal representation of fermionic wavefunctions (fermions= bosons+ one), *arXiv preprint arXiv:2510.11431* (2025).

[22] L. Fu, Fermi sets: Universal and interpretable neural architectures for fermions, *arXiv preprint arXiv:2601.02508* (2026).

[23] Y. Qian, T. Zhao, J. Zhang, T. Xiang, X. Li, and J. Chen, Describing landau level mixing in fractional quantum hall states with deep learning, *Physical Review Letters* **134**, 176503 (2025).

[24] I. Sodemann and A. MacDonald, Landau level mixing and the fractional quantum hall effect, *Physical Review B—Condensed Matter and Materials Physics* **87**, 245425 (2013).

[25] C. Wang, A. Gupta, P. T. Madathil, S. K. Singh, Y. J. Chung, L. N. Pfeiffer, K. W. Baldwin, and M. Shayegan, Next-generation even-denominator fractional quantum hall states of interacting composite fermions, *Proceedings of the National Academy of Sciences* **120**, e2314212120 (2023).

[26] A. Tsukazaki, S. Akasaka, K. Nakahara, Y. Ohno, H. Ohno, D. Maryenko, A. Ohtomo, and M. Kawasaki, Observation of the fractional quantum hall effect in an oxide, *Nature materials* **9**, 889 (2010).

[27] Q. Shi, E.-M. Shih, M. V. Gustafsson, D. A. Rhodes, B. Kim, K. Watanabe, T. Taniguchi, Z. Papić, J. Hone, and C. R. Dean, Odd-and even-denominator fractional quantum hall states in monolayer wse2, *Nature Nanotechnology* **15**, 569 (2020).

[28] A. C. Archer and J. K. Jain, Static and dynamic properties of type-ii composite fermion wigner crystals, *Physical Review B—Condensed Matter and Materials Physics* **84**, 115139 (2011).

[29] H. Yi and H. Fertig, Laughlin-jastrow-correlated wigner crystal in a strong magnetic field, *Physical Review B* **58**, 4019 (1998).

[30] R. Narevich, G. Murthy, and H. Fertig, Hamiltonian theory of the composite-fermion wigner crystal, *Physical Review B* **64**, 245326 (2001).

[31] C.-C. Chang, G. S. Jeon, and J. K. Jain, Microscopic verification of topological electron-vortex binding in the lowest landau-level crystal state, *Physical review letters* **94**, 016809 (2005).

[32] A. C. Archer, K. Park, and J. K. Jain, Competing crystal phases in the lowest landau level, *Physical review letters* **111**, 146804 (2013).

[33] Z. Tesanovic, F. Axel, and B. Halperin, “hall crystal”versus wigner crystal, *Physical Review B* **39**, 8525 (1989).

[34] X. Wan, E. Rezayi, and K. Yang, Edge reconstruction in the fractional quantum hall regime, *Physical Review B* **68**, 125307 (2003).

[35] X.-G. Wen and A. Zee, Shift and spin vector: New topological quantum numbers for the hall fluids, *Physical review letters* **69**, 953 (1992).

[36] See Supplementary Material for additional details.

[37] F. D. M. Haldane, Many-particle translational symmetries of two-dimensional electrons at rational landau-level filling, *Phys. Rev. Lett.* **55**, 2095 (1985).

[38] F. D. M. Haldane and E. H. Rezayi, Periodic laughlin-jastrow wave functions for the fractional quantized hall effect, *Phys. Rev. B* **31**, 2529 (1985).

[39] M. Fremling, Coherent state wave functions on a torus with a constant magnetic field, *Journal of Physics A: Mathematical and Theoretical* **46**, 275302 (2013).

[40] F. Haldane, A modular-invariant modified weierstrass sigma-function as a building block for lowest-landau-level wavefunctions on the torus, *Journal of Mathematical Physics* **59** (2018).

[41] F. Haldane, The origin of holomorphic states in landau levels from non-commutative geometry and a new formula for their overlaps on the torus, *Journal of Mathematical Physics* **59** (2018).

[42] J. Wang, S. D. Geraedts, E. Rezayi, and F. Haldane, Lattice monte carlo for quantum hall states on a torus, *Physical Review B* **99**, 125123 (2019).

[43] I. von Glehn, J. S. Spencer, and D. Pfau, A self-attention ansatz for ab-initio quantum chemistry, *arXiv preprint arXiv:2211.13672* (2022).

[44] A. P. Fadon, D. Pfau, J. S. Spencer, W. T. Lou, T. Neupert, and W. Foulkes, Extracting anyon statistics from neural network fractional quantum hall states, *arXiv preprint arXiv:2512.15872* (2025).

[45] B. Halperin, Z. Tesanovic, and F. Axel, Compatibility of crystalline order and the quantized hall effect, *Physical Review Letters* **57**, 922 (1986).

[46] G. Murthy, Hall crystal states at $\nu = 2$ and moderate landau level mixing, *Physical Review Letters* **85**, 1954 (2000).

[47] S. Kivelson, C. Kallin, D. P. Arovas, and J. R. Schrieffer, Cooperative ring exchange theory of the fractional quantized hall effect, *Physical review letters* **56**, 873 (1986).

[48] N. Paul, Y. Zhang, and L. Fu, Giant proximity exchange and flat chern band in 2d magnet-semiconductor heterostructures, *Science Advances* **9**, eabn1401 (2023).

[49] F. Wu, T. Lovorn, E. Tutuc, I. Martin, and A. MacDonald, Topological insulators in twisted transition metal dichalcogenide homobilayers, *Physical review letters* **122**, 086402 (2019).

[50] N. Morales-Durán, N. Wei, J. Shi, and A. H. MacDonald, Magic angles and fractional chern insulators in twisted homobilayer transition metal dichalcogenides, *Physical Review Letters* **132**, 096602 (2024).

[51] J. Shi, N. Morales-Durán, E. Khalaf, and A. H. MacDonald, Adiabatic approximation and aharonov-casher bands in twisted homobilayer transition metal dichalcogenides, *Physical Review B* **110**, 035130 (2024).

[52] A. Vaswani, N. Shazeer, N. Parmar, J. Uszkoreit, L. Jones, A. N. Gomez, L. Kaiser, and I. Polosukhin, Attention is all you need, *Advances in neural information processing systems* **30** (2017).

Supplementary material for: “First-Principles AI finds crystallization of fractional quantum Hall liquids”

Ahmed Abouelkomsan¹ and Liang Fu¹

¹*Department of Physics, Massachusetts Institute of Technology, Cambridge, MA-02139, USA*

In the supplementary material, we provide additional details about magnetic boundary conditions, the neural network architecture, optimization and a table of the variational energies we obtain.

Appendix A: Magnetic Boundary Conditions

Consider a quantum system subject to a magnetic field

$$B(\mathbf{r}) = B_0 + \delta B(\mathbf{r}), \quad (\text{A1})$$

where B_0 is the uniform (spatially averaged) component and $\delta B(\mathbf{r})$ fluctuates in space but averages to zero over the system. Introducing a vector potential via $B(\mathbf{r}) = \nabla \times \mathbf{A}(\mathbf{r})$, it is natural to decompose

$$\mathbf{A}(\mathbf{r}) = \mathbf{A}_0(\mathbf{r}) + \delta \mathbf{A}(\mathbf{r}), \quad \nabla \times \mathbf{A}_0 = B_0, \quad (\text{A2})$$

where $\mathbf{A}_0(\mathbf{r})$ is linear in \mathbf{r} in any gauge.

We now impose periodic boundary conditions by placing the system on a torus spanned by two basis vectors \mathbf{L}_1 and \mathbf{L}_2 . Let $\mathbf{L} = m\mathbf{L}_1 + n\mathbf{L}_2$ be a generic lattice vector with integers m, n . In the presence of a net magnetic flux through the torus, the vector potential $\mathbf{A}(\mathbf{r})$ cannot be strictly periodic under translations by \mathbf{L} due to the linear in \mathbf{r} part $\mathbf{A}_0(\mathbf{r})$,

$$\mathbf{A}(\mathbf{r} + \mathbf{L}) \neq \mathbf{A}(\mathbf{r}), \quad (\text{A3})$$

On the other hand physical observables must remain invariant under $\mathbf{r} \mapsto \mathbf{r} + \mathbf{L}$. This invariance is therefore enforced by allowing a translation around the torus to be accompanied by a position-dependent phase of the wavefunction,

$$\psi(\mathbf{r} + \mathbf{L}) = e^{i\xi_{\mathbf{L}}(\mathbf{r})} \psi(\mathbf{r}). \quad (\text{A4})$$

Assuming the Hamiltonian depends on \mathbf{A} only through minimal coupling $\mathbf{p} \rightarrow \boldsymbol{\pi} = -i\hbar\nabla + e\mathbf{A}(\mathbf{r})$, gauge covariance of the kinetic term implies $\boldsymbol{\pi}(\mathbf{r} + \mathbf{L}) e^{i\xi_{\mathbf{L}}(\mathbf{r})} = e^{i\xi_{\mathbf{L}}(\mathbf{r})} \boldsymbol{\pi}(\mathbf{r})$, so that $\xi_{\mathbf{L}}(\mathbf{r})$ compensates the change of \mathbf{A} under translation. In other words, a torus translation must be accompanied by a gauge transformation so that the Hamiltonian remains gauge-covariant; this requirement determines $\xi_{\mathbf{L}}(\mathbf{r})$,

$$\nabla \xi_{\mathbf{L}}(\mathbf{r}) = \frac{e}{\hbar} [\mathbf{A}(\mathbf{r} + \mathbf{L}) - \mathbf{A}(\mathbf{r})]. \quad (\text{A5})$$

The boundary phases $\xi_{\mathbf{L}}(\mathbf{r})$ cannot be chosen independently: they must be mutually consistent when we traverse the torus along different paths. In particular, translating by \mathbf{L}_1 and then \mathbf{L}_2 must bring the wavefunction to the same physical state as translating by \mathbf{L}_2 and then \mathbf{L}_1 . Using $\psi(\mathbf{r} + \mathbf{L}) = e^{i\xi_{\mathbf{L}}(\mathbf{r})} \psi(\mathbf{r})$, we obtain,

$$\psi(\mathbf{r} + \mathbf{L}_1 + \mathbf{L}_2) = e^{i\xi_{\mathbf{L}_2}(\mathbf{r} + \mathbf{L}_1)} e^{i\xi_{\mathbf{L}_1}(\mathbf{r})} \psi(\mathbf{r}), \quad (\text{A6})$$

$$\psi(\mathbf{r} + \mathbf{L}_2 + \mathbf{L}_1) = e^{i\xi_{\mathbf{L}_1}(\mathbf{r} + \mathbf{L}_2)} e^{i\xi_{\mathbf{L}_2}(\mathbf{r})} \psi(\mathbf{r}). \quad (\text{A7})$$

Consistency therefore requires the ratio of these two phases to be unity,

$$\exp \left\{ i[\xi_{\mathbf{L}_2}(\mathbf{r} + \mathbf{L}_1) + \xi_{\mathbf{L}_1}(\mathbf{r}) - \xi_{\mathbf{L}_1}(\mathbf{r} + \mathbf{L}_2) - \xi_{\mathbf{L}_2}(\mathbf{r})] \right\} = 1. \quad (\text{A8})$$

Taking a gradient and using equation (A5), we find,

$$\xi_{\mathbf{L}_2}(\mathbf{r} + \mathbf{L}_1) + \xi_{\mathbf{L}_1}(\mathbf{r}) - \xi_{\mathbf{L}_1}(\mathbf{r} + \mathbf{L}_2) - \xi_{\mathbf{L}_2}(\mathbf{r}) = \frac{e}{\hbar} \oint_{\partial\square} \mathbf{A} \cdot d\ell = \frac{e}{\hbar} \int_{\square} B(\mathbf{r}) d^2r \equiv \frac{e}{\hbar} \Phi. \quad (\text{A9})$$

Where \square denotes the torus and $\partial\square$ denotes the boundary of the torus. Equation (A8) then becomes $\exp(i\frac{e}{\hbar}\Phi) = 1$, which implies

$$\Phi = N_{\phi} \frac{h}{e}, \quad N_{\phi} \in \mathbb{Z}, \quad (\text{A10})$$

i.e., the total magnetic flux through the torus must be an integer multiple of the flux quantum.

Moreover, the magnetic boundary condition (Eq. (A4) implies that transporting a particle around the torus returns the wavefunction to itself only up to a phase. The net phase accumulated around the boundary of the torus \square is

$$\Delta\varphi = \frac{e}{\hbar} \oint_{\partial\square} \mathbf{A} \cdot d\ell = \frac{e}{\hbar} \Phi = 2\pi N_\phi, \quad (\text{A11})$$

The single particle wavefunction therefore carries an integer total vorticity set by the number of flux quanta N_ϕ .

For the wavefunction to be continuous, the net winding necessarily implies the existence of zeros of in the fundamental domain of the torus. The winding around a zero can be either positive (vortex) or negative (anti-vortex) but the total winding is equal to N_ϕ . Let N_z be the number of vortices and $N_{\bar{z}}$ be the number of anti-vortices with negative winding. Assuming $B_0 > 0$, we have

$$N_\phi = N_z - N_{\bar{z}} \quad (\text{A12})$$

Around a vortex, a complex function $f(z, \bar{z}) \sim z^n$ for some integer n . Similarly, for an anti-vortex, $f(z, \bar{z}) \sim \bar{z}^n$. Taking case of the lowest landau level (LLL) where the wavefunction is holomorphic (up to a Gaussian factor), we immediately see that any LLL wavefunction has N_ϕ zeros.

In addition to position-dependent magnetic phases $\xi_{\mathbf{L}}(\mathbf{r})$ due to the existence of net flux, the wavefunction can acquire a twist phase $e^{i\varphi}$ under translations, corresponding to threading a flux through the handles of the torus which is implemented by a *constant* vector potential.

The above discussions generalizes readily for a many-body system. In this case, the wavefunction of N particles transforms as,

$$\Psi(\mathbf{r}_1, \dots, \mathbf{r}_i + \mathbf{L}, \dots, \mathbf{r}_N) = e^{i\varphi} e^{i\xi_{\mathbf{L}}(\mathbf{r}_i)} \Psi(\mathbf{r}_1, \dots, \mathbf{r}_N) \quad (\text{A13})$$

under torus translations of any particle \mathbf{r}_i .

Appendix B: Neural Network Architecture

In this section, we describe the MagNet architecture used throughout the paper. We use an architecture that is schematically shown in Fig. 1 in the main text and has both self-attention and multilayer perceptron components. As we are working with a torus supercell, we use periodic features for each particle. First a feature vector $f_i \equiv f(\mathbf{r}_i)$ is defined for the i -th particle as

$$\mathbf{f}_i \equiv f(\mathbf{r}_i) = \begin{pmatrix} \cos(\mathbf{G}_1 \cdot \mathbf{r}_i) \\ \cos(\mathbf{G}_2 \cdot \mathbf{r}_i) \\ \sin(\mathbf{G}_1 \cdot \mathbf{r}_i) \\ \sin(\mathbf{G}_2 \cdot \mathbf{r}_i) \end{pmatrix} \quad (\text{B1})$$

where \mathbf{G}_a ($a = 1, 2$) denote the two supercell reciprocal vectors $\mathbf{G}_a \cdot \mathbf{L}_b = 2\pi\delta_{ab}$ with \mathbf{L}_a ($a = 1, 2$) are the two basis vector of the torus. This feature vector represent a periodized version of the particle coordinates. Each feature vector is then mapped to an initial \mathbf{h}_i^0 vector which lives in a higher dimensional space through a transformation,

$$\mathbf{h}_i^0 = W^0 \mathbf{f}_i \quad (\text{B2})$$

with $W^0 \in \mathbb{R}^{d_L} \times \mathbb{R}^{2d_{\text{dim}}}$ with d_L is the dimension of the higher dimensional space where the particle coordinates are embedded which corresponds to the width of the internal layers of the neural network. d_{dim} is the spatial dimension ($d_{\text{dim}} = 2$ in our case). Importantly, W^0 is the same for each particle coordinate. Having mapped the coordinates of all particles to vectors $\{\mathbf{h}_i^0\}$, these vectors undergo two different types of transformations, multi-head self attention followed by multilayer perceptron (MLP) which we explain next.

1. Multilayer Perceptron (MLP)

MLPs are standard feed-forward neural networks that implements the following transformation on a *generic* vector $\mathbf{g}_1 \in \mathbb{R}^{d_L}$ to yield another vector \mathbf{g}_2 ,

$$\mathbf{g}_2 = \mathbf{g}_1 + F(W\mathbf{g}_1 + \mathbf{b}) \quad (\text{B3})$$

with W is a linear transformation $W \in \mathbb{R}^{d_L} \times \mathbb{R}^{d_L}$ and $\mathbf{b} \in \mathbb{R}^{d_L}$ is a bias vector. F here represents a non-linear activation function which we choose to be the GELU function.

2. Self-attention

In the NN architecture (Fig. 1 in the main text), MLPs act individually on each particle without mixing different particle streams which cannot describe correlations between particles. In order to capture such correlations, we utilize the self-attention mechanism [52] which form the basis of transformers used in large language models. Self-attention mechanism learns how each particle is influenced by the remaining particles. Self attention acts of all set of particle streams in the l -layer $\{\mathbf{h}_i^l\}$ to generate intermediate streams $\{\mathbf{g}_i^l\}$ that are then passed to the MLP (B3). Schematically we have the following,

$$\cdots \rightarrow \{\mathbf{h}_i^l\} \xrightarrow{\text{SELF-ATTN}} \{\mathbf{g}_i^l\} \xrightarrow{\text{PERCEPTRON}} \{\mathbf{h}_i^{l+1}\} \rightarrow \cdots \quad (\text{B4})$$

In the self-attention mechanism, three features for each element in $\{h_i^l\}$ are defined which are called *keys*, *queries* and *values* and are defined as,

$$\mathbf{k}_i^{lh} = W_k^{lh} \mathbf{h}_i^l, \quad W_k^{lh} \in \mathbb{R}^{d_{\text{attn}}} \times \mathbb{R}^{d_L} \quad (\text{B5})$$

$$\mathbf{q}_i^{lh} = W_q^{lh} \mathbf{h}_i^l, \quad W_q^{lh} \in \mathbb{R}^{d_{\text{attn}}} \times \mathbb{R}^{d_L} \quad (\text{B6})$$

$$\mathbf{v}_i^{lh} = W_v^{lh} \mathbf{h}_i^l, \quad W_v^{lh} \in \mathbb{R}^{d_{\text{attnvals}}} \times \mathbb{R}^{d_L} \quad (\text{B7})$$

The transformations $\{W_k^{lh}, W_q^{lh}, W_v^{lh}\}$ are the same for each particle i . We use multi-head attention where more than one self-attention operation is applied, indexed by h in W_k^{lh} , W_q^{lh} and W_v^{lh} which is not to be confused with the particle stream vectors \mathbf{h}_i^l . The dimensions d_{attn} and d_{attnvals} are different from d_L and are generally much smaller. The keys and queries vectors have the same vector space dimension d_{attn} to allow for comparison between two different particle streams i, j through the dot product $\mathbf{k}_i^{lh} \cdot \mathbf{q}_j^{lh}$. The values \mathbf{v}_i^{lh} is a measure of the influence on particle i from the remaining particles $j \neq i$. The value of self-attention for each particle i is computed as

$$\text{SELFATTN}_i(\{\mathbf{h}_j^l\}; W_k^{lh}, W_q^{lh}, W_v^{lh}) = \frac{1}{N} \sum_{j=1}^N \exp(\mathbf{k}_i^{lh} \cdot \mathbf{q}_j^{lh}) \mathbf{v}_j^{lh} \quad (\text{B8})$$

with a normalization factor,

$$\mathcal{N} = \sqrt{d_{\text{attnvals}}} \sum_{j=1}^N \exp(\mathbf{k}_i^{lh} \cdot \mathbf{q}_j^{lh}) \quad (\text{B9})$$

The physical meaning of (B8) is transparent. The self-attention value of particle i returns the value \mathbf{v}_j^{lh} of particle stream j weighted by the exponential factor which measures the correlations between i, j such that the most relevant particles j for each particle j are identified. The intermediate streams are given by

$$\mathbf{g}_i^{l+1} = \mathbf{h}_i^l + W_o^l \text{concat}_h [\text{SELFATTN}_i(\{\mathbf{h}_j^l\}; W_k^{lh}, W_q^{lh}, W_v^{lh})] \quad (\text{B10})$$

All values of self-attention from the multi-head attention are concatenated then transformed through transformation $W_0^l \in \mathbb{R}^{d_L} \times \mathbb{R}^{N_{\text{heads}} \times \text{attnvals}}$. The intermediate streams $\{\mathbf{g}_i^l\}$ are passed through MLP giving rise to,

$$\mathbf{h}_i^{l+1} = \mathbf{g}_i^l + F(W^l \mathbf{g}_i^l + \mathbf{b}^{l+1}) \quad (\text{B11})$$

Here W^l and \mathbf{b}^l are the same for all particle streams which are labeled by i .

3. Projection onto $N \times N_{\text{det}}$ amplitudes

The final output of the neural network $\{\mathbf{h}_i^L\}$ is projected onto $N \times N_{\text{det}}$ distinct sets of amplitudes

$$F_j^n(\mathbf{r}_i; \{\mathbf{r}_{\neq i}\}) = \mathbf{w}_{2j}^n \cdot \mathbf{h}_i^L + i \mathbf{w}_{2j+1}^n \cdot \mathbf{h}_i^L \quad (\text{B12})$$

with $j = 1, \dots, N$ and $n = 1, \dots, N_{\text{det}}$. \mathbf{w}_{2j}^n and \mathbf{w}_{2j+1}^n are projection matrices that construct the real and the imaginary part of F_j^n . It is important to note that in order for the full ansatz to describe a fermionic anti-symmetric wavefunction, the amplitudes $F_j^n(\mathbf{r}_i; \{\mathbf{r}_{\neq i}\})$ are chosen to be permutation invariant in the coordinates $\{\mathbf{r}_{\neq i}\}$,

$$F_j^n(\mathbf{r}_i; \{\mathbf{r}_k, \dots, \mathbf{r}_l, \dots\}) = F_j^n(\mathbf{r}_i; \{\mathbf{r}_l, \dots, \mathbf{r}_k, \dots\}) \quad (\text{B13})$$

for $k, l \neq i$. This property is inherited from the form of the self-attention operations (B8).

Parameter	Value
Architecture	
Network layers	$L = 4$
Attention heads per layer	$N_{\text{heads}} = 4$
Attention dimension	$d_{\text{attn}} = d_{\text{attnvals}} = 64$
Perceptron dimension	$d_L = 256$
# perceptrons per layer	2
Determinants	$N_{\text{det}} = 2$
Layer norm	True
Activation	GELU
Training	
Training iterations	$15e6 - 20e6$
Learning rate (fixed)	$\eta_0 = 0.1$
Optimizer	KFAC
MCMC	
Batch size	1024
Initial move width	0.2
KFAC	
Norm constraint	1×10^{-4}
Damping	1×10^{-3}
L_2 regularization	0.0
Momentum	0.0

TABLE I. Table of default hyperparameters used in our numerical calculations with the MagNet architecture.

4. Projection onto $N_\phi \times N \times N_{\text{det}}$ winding maps

In addition to the set of amplitudes F_j^n , the final output of the neural network is projected to construct the winding maps $\eta_j^{(n,\alpha)}$ as symmetric many-body functions,

$$\eta_j^{(n,\alpha)}(\{\mathbf{r}\}) = \frac{1}{N} \sum_{i=1,\dots,N} \boldsymbol{\omega}_{2j}^{(n,\alpha)} \cdot \mathbf{h}_i^L + i \boldsymbol{\omega}_{2j+1}^{(n,\alpha)} \cdot \mathbf{h}_i^L \quad (\text{B14})$$

with $i = 1, \dots, N$, $n = 1, \dots, N_{\text{det}}$ and $\alpha = 1, \dots, N_\phi$. $\boldsymbol{\omega}_{2j}^{(n,\alpha)}$ and $\boldsymbol{\omega}_{2j+1}^{(n,\alpha)}$ are two projection matrices that construct the real and imaginary part of the complex coordinate of the zero.

The sum of the winding maps, $\bar{\eta}_j^{(n)} = (\sum_\alpha \eta_j^{(n,\alpha)}) \bmod (L_x + iL_y)$, fixes the twist phase φ in Eq. (A13) [42]. We choose a twist phase of $\varphi = 0$ by imposing that $\eta_j^{(n)} = 0$ by first obtaining $\eta_j^{(n,\alpha)}(\{\mathbf{r}\})$ and subtracting it from its mean over α .

Appendix C: Optimization

In Table I, we list the hyperparameters of the neural network we used in our work. We particularly note the small norm constraint we use in order to stabilize the training. We initialize the training in two different ways. For $\kappa = 3$ and $\kappa = 9$, we do a random initialization while for $\kappa = 12, 15, 20$, we initialize from the optimized phase at either $\kappa = 3$ or $\kappa = 9$. We find that initializing from the optimized FQH phase to accelerate convergence, even when the ground state exhibit crystalline correlations. We checked in various cases that both random initialization and initialization from the optimized FQH liquid give the same result.

Fig. S1 shows a representative training curve for $N = 12$ and $N_\phi = 36$ flux quantum at $\kappa = 3.0$

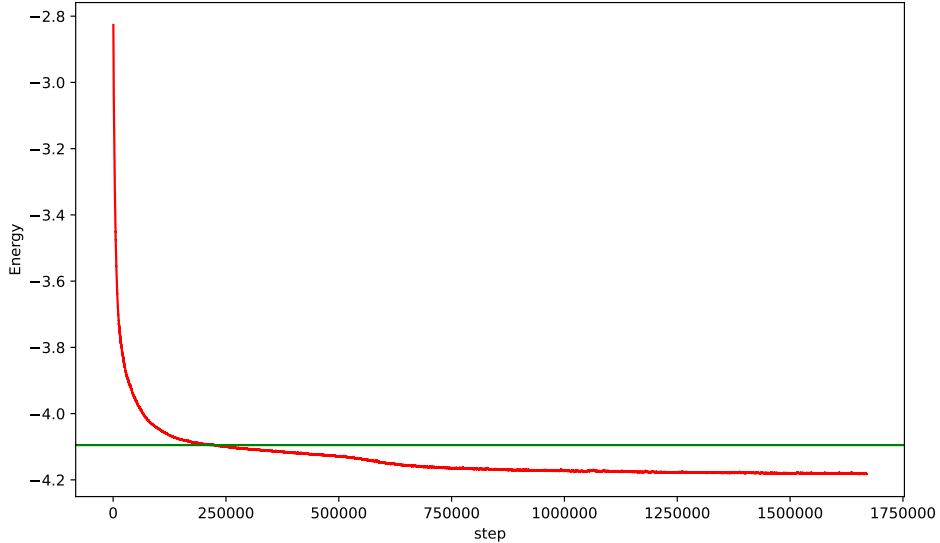


FIG. S1. Training curve for $N = 12$ and $N = 36$ at $\kappa = 3.0$ with random initialization. Energy at a given step is averaged over the previous 4000 steps and it is in units of $\hbar\omega_c$ and does not include the Madelung constant of this finite torus. The green line denotes the energy of the lowest landau level projected ED.

Appendix D: Table of Energies

Below, we list the energies we obtained for various Landau level mixing κ for both $N = 9$ and $N = 12$. We measure energies in units of $\hbar\omega_c$. To facilitate comparison with exact diagonalization, we do not include the Madelung constant in the table below.

Landau level mixing	$N = 9$	$N = 12$
$\kappa = 3$	-2.61141(27)	-4.18057(20)
$\kappa = 9$	-17.24265(11)	-25.06976(21)
$\kappa = 12$	-24.680162(89)	-35.66683(21)
$\kappa = 15$	-32.167333(99)	-46.35916(16)
$\kappa = 20$	-44.753212(87)	-64.29958(12)